Research Article | Vol. 29, No. 10 / 10 May 2021 / Optics Express 14841

Optics EXPRESS

Enhanced microLED efficiency via strategic pGaN contact geometries

KEITH BEHRMAN[1,*] AND IOANNIS KYMISSIS[1,2]

[1]Electrical Engineering Department, Columbia University, New York City, NY 10027, USA
[2]Lumiode, The Bronx, NY 10451, USA
[*]keith.behrman@columbia.edu

Abstract: Micro light-emitting diode (microLED) structures were modeled and validated with fabricated devices to investigate p-type GaN (pGaN) contact size dependence on power output efficiency. Two schemes were investigated: a constant 10 μm diameter pGaN contact and varying microLED sizes and a constant 10 μm diameter microLED with varying contact sizes. Modeled devices show a 17% improvement in output power by increasing the microLED die size. Fabricated devices followed the same trend with a 70% improvement in power output. Modeled microLED devices of a constant size and varying inner contact sizes show optimized power output at different current densities for various contact sizes. In particular, lower current densities show optimized output for smaller pGaN contacts and trend towards larger contacts for higher current densities in a balance between undesirable efficiency losses at high-current injection and preventing surface recombination losses. We show that for all device geometries, it is preferential to shrink the pGaN contact to maximize efficiency by suppressing surface recombination losses and further improvements should be carefully considered to optimize efficiency for a desired operational brightness.

1. Introduction

Micro light-emitting diode (microLED) displays are rapidly progressing to the forefront of display technologies due to their extraordinary characteristics. MicroLEDs can outperform liquid-crystal displays (LCD) and organic light-emitting diode (OLED) displays in brightness, ambient contrast ratios, pixel response time, and minimum emitter size [1]. These strengths pose microLEDs in the forefront for augmented reality (AR) and mixed reality (MR) near-to-eye displays (NED) where the display requires small emitters with brightness that compete with sunlight. However, several challenges still prevent microLED technologies from widespread use. Red, blue, and green pixel integration remains a key challenge while the overall cost and yield requirements for mass-transfer methods are still prohibitively high [2,3].

For GaN/InGaN microLEDs, efficiency rapidly decreases at higher current densities with smaller emitter sizes, commonly referred to as microLED droop [4,5]. Several studies have investigated the causes of microLED droop and analytical models have been proposed to account for droop with decreasing size [6–11]. One of the main contributing factors to the decreasing performance with smaller emitters is non-radiative surface recombination due to nitrogen vacancies which creates Shockley-Read-Hall (SRH) trap sites from dry-etched GaN/InGaN during mesa formation [12–14]. The smaller emitter sizes increases the sidewall surface-area-to-emitter-size ratio, thus allowing injected current to more readily diffuse towards the sidewalls increasing surface recombination current relative to radiative current [10]. For AR/MR display applications that require extremely small microLED emitters, these efficiency losses become increasingly prohibitive to light output and power efficiency.

Several techniques have been described to mitigate these efficiency roll-offs. Methods have been proposed to minimize the amount of sidewall damage in dry etched pixels by altering plasma gas concentrations and plasma power [15]. Wet etching techniques have also been investigated

#425800 https://doi.org/10.1364/OE.425800
Journal © 2021 Received 22 Mar 2021; revised 19 Apr 2021; accepted 19 Apr 2021; published 28 Apr 2021

Optics EXPRESS

and compared to dry-etching methods [16,17]. Solution treatment to partially etch or clean the sidewalls have also been proposed to passivate the etched microLED surface after dry etching to improve device performance [18]. The microLED sidewalls are often coated with an insulating material during fabrication to allow for lithographically patterned deposited metal to electrically contact the pGaN layer without shorting the device. To this end, different insulators have been investigated for their ability to partially passivate the etched microLED sidewalls and improve device performance [19]. While these methods do improve device performance, they do not completely offset non-radiative current losses to surface recombination.

A second cause of efficiency droop in LEDs, independent of emitter size, stems from increased non-radiative recombination and leakage current effects at high operational current densities [6,20]. The exact cause of high current droop has been contested and several models have been proposed to account for diminishing efficiencies [21]. Auger recombination has been shown to be a temperature-dependent source of non-radiative recombination partially responsible for efficiency droop [22]. A secondary source of droop occurs at high-injection current conditions and may partially be caused by Auger recombination and further explained by a modified drift-leakage model [23]. Moreover, SRH recombination from trap states unrelated to etched sidewalls is temperature dependent and thus efficiency decreases as the device heats up to operating temperature if effective heat-sinking is not employed [24–26]. The exact interplay of these efficiency losses is beyond the scope of this paper and several review articles on the matter are cited [21,27,28].

MicroLED structures are often dry-etched with a nickel hardmask due to nickel's resistance to the chlorine-based plasma used in dry etching GaN [29]. Nickel is also an excellent metal choice for good ohmic contact to p-type GaN (pGaN) [30–32]. Thus, nickel is often employed as both the dry-etch mask and the ohmic conctact for a single lithographic self-aligned microLED process step [33]. The self-alignment method is favorable in reducing the number of lithographic steps needed to form a device and it also creates perfect alignment and coverage of the entire exposed pGaN, allowing for the maximum amount of possible current injection with minimal series contact resistance. However, for small microLED devices, this work proposes that self-aligned contacts are overall detrimental to device performance and there are simple application-dependent methods to optimally reshape the pGaN contact to optimize device performance. Previous studies have found a contact geometry dependence on current spreading and light output in vertical, chip-sized LED structures, but no substantial work has been completed on contact geometry in microLED devices [34].

This work examines microLED performance and efficiency for emitters ranging in size from 10 to 20 μm in diameter. Within these devices, the pGaN contact diameter is also investigated to understand the effect of minimizing sidewall recombination and the interplay with current crowding efficiency losses. Efficiency is modeled with a hybrid approach: 1D drift-diffusion modeling of the bandgap structure from epitaxial growth parameters and 3D modeling of the current spreading, internal heating, and efficiency of the device structures. Modeling results are discussed in detail and verified by fabricated devices of the same structure and similar material parameters.

2. Experimental methods

2.1. Device fabrication and testing

LED wafers of epitaxially grown GaN/InGaN on patterned sapphire substrates as shown in Fig. 1(a) were used for this study. Devices were fabricated according to the schematic in Fig. 1(b). First, pGaN contacts (20 nm Ni and 50 nm Au) were electron-beam evaporated and lithographically patterned via lift-off. MicroLED dimensions of various sizes according to Fig. 1(c) were defined by lithographically patterning Megaposit SPR220 4.5 photoresist as a dry-etch mask. MicroLEDs were etched in an Oxford PlasmaPro 100 Cl-etcher using Cl/BCl_3

Optics EXPRESS

(a)

pGaN:Mg	100 nm	Mg: $1.2x10^{19}$
pAlGaN	50 nm	Mg: $1.4x10^{20}$
GaN	5 nm	N/A
InGaN	3.5 nm	"blue"
uGaN	350 nm	Si: $1.5x10^{17}$
nGaN	2.0 µm	Si: $1.0x10^{19}$
nAlGaN	100 nm	Si: $1.0x10^{19}$
nGaN	500 nm	Si: $5.0x10^{18}$
uGaN	2.5 µm	N/A
patterned sapphire		

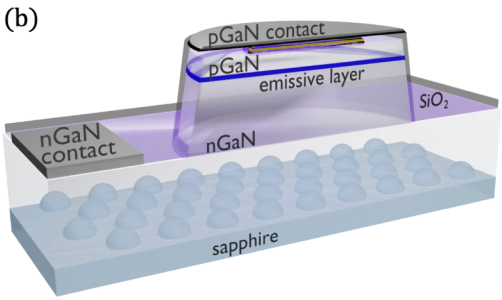

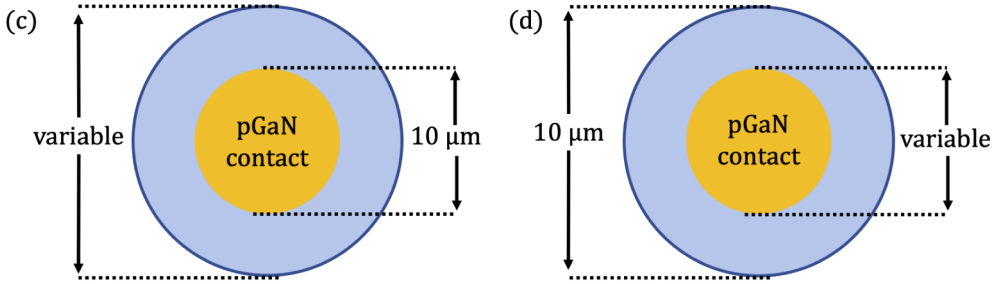

Fig. 1. (a) Material, thickness, and doping concentration of the LED epitaxial stack grown on dimple-patterned sapphire. (b) Schematic cross-section of the fabricated devices. (c) Devices examined had a constant 10 μm pGaN contact diameter and variable pixel diameter ranging from 10 to 20 μm. (d) Inversely from c, devices examined had a constant 10 μm microLED diameter and a pGaN contact diameter ranging from 4 to 10 μm.

to an approximate depth of 1200 nm. n-type GaN (nGaN) contacts (80 nm Al) were thermally deposited and lithographically patterned via lift-off. An insulating SiO_2 layer (500 nm) was deposited via plasma-enhanced chemical vapor deposition (PECVD) in an Oxford PlasmaPro 80. Via holes were lithographically patterned with SPR220 4.5 and dry-etched with a CHF_3 plasma in an Oxford PlasmaPro 100. Finally, aluminum interconnects to the nGaN and pGaN were sputter-deposited in an AJA sputter system. The aluminum was patterned and dry-etched in a Cl/BCl_3 plasma. The aluminum was designed uniformly larger than the microLED pixels to also act as a reflective mirror focusing light out the bottom. Finally, probe pads were deposited and patterned with e-beam metal evaporation (10 nm Cr / 500 nm Au).

Luminance-current-voltage (LIV) measurements were recorded with a Keithley 2600 and a ThorLabs S120VC power meter. pGaN and nGaN contact pads were probed by micromanipulators with the microLED under test centered above the photodiode recording bottom emissive light through the sapphire substrate. External quantum efficiency (EQE) measurements are not exact as some amounts of stray light were lost due to substrate modes and imperfect out-coupling. However, the relative size of the microLEDs (10 to 20 μm diameter) compared to the photodiode size (10 mm diameter) ensures that there is no substantial difference between different device sizes and EQE measurements can be quantitatively compared.

2.2. *Modeling methods*

Devices were modeled using STR-Software's SiLENSe and SpeCLED tools. Material properties from Table 1 were modeled with SiLENSe to generate a 1D bandgap model, electrical properties, and internal quantum efficiencies (IQE) from 300 to 500 K. The output data from SiLENSe was then transferred to SpeCLED where several different microLED models were constructed

Optics EXPRESS

according to Fig. 1(c) and (d). Each model was solved for current densities ranging from approximately 10 to 3000 A/cm^2. SpecLED was configured to self-consistently solve current spreading, self-heating effects, and IQE per mesh cell. Surface recombination current was also solved for assuming a surface recombination velocity of 1x10^5 cm/s^2 [11]. This recombination velocity is an estimate based on the higher range of reported InGaN and GaN recombination velocities. Average IQE, total emission power, emission power densities, and current-voltage characteristics were recorded for each model and compared. More details on modeling methodology can be found here [35,36].

3. Results

3.1. Constant pGaN contact diameter with variable pixel sizes

Experimental microLED devices were fabricated, measured, and compared to simulation results according to Fig. 1(c). Figure 2 shows modeled device results from SpeCLED. Output power, IQE, surface recombination current, and the ratio of surface recombination current to total operational current are plotted against current density. Datapoints were recorded for current densities ranging from approximately 20 to 3000 A / cm^2 with the 10 μm diameter pGaN contact used to define area for comparison consistency. However, note that current densities then vary

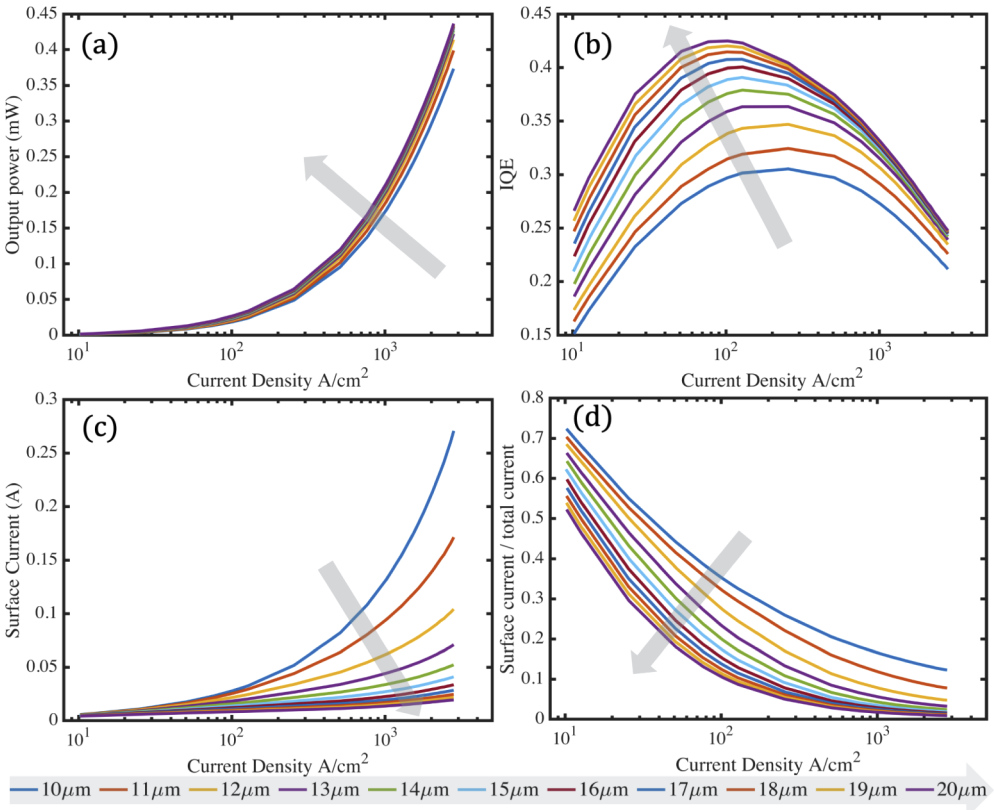

Fig. 2. Modeled device results for a constant 10μm pGaN contact diameter and varying microLED pixel diameters as depicted in Fig. 1(c). The grey arrows point in the trend of larger microLED sizes. (a) Output power versus current density. (b) IQE versus current density. (c) Surface recombination current versus current density. (d) Ratio of surface recombination current to total operational current versus current density.

Optics EXPRESS

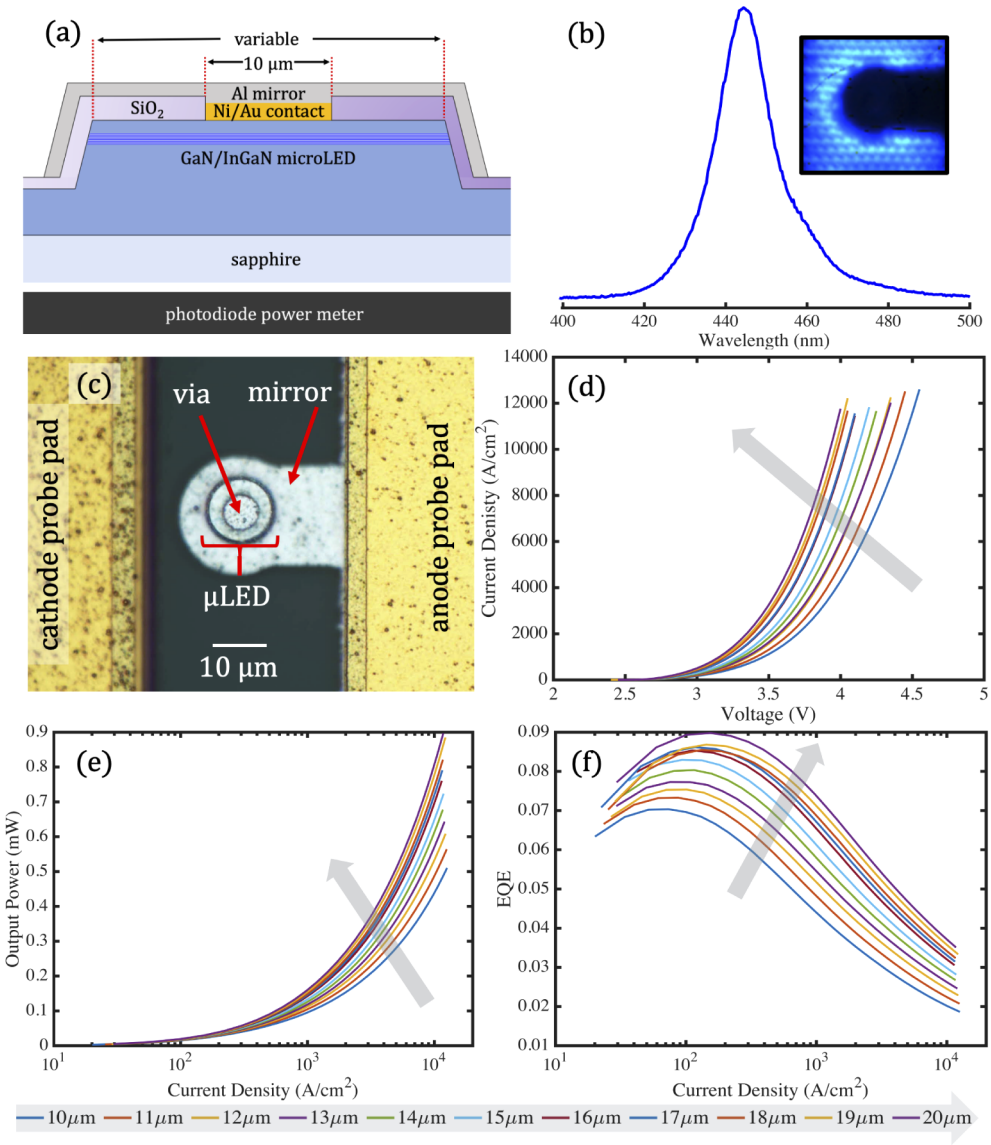

Fig. 3. Measured results for fabricated microLEDs with a 10 μm pGaN contact diameter and varying microLED pixel diameters as depicted in Fig. 1(c). (a) A cross-sectional schematic of the device and measurement setup. Light was measured from the bottom of the microLED through the sapphire substrate. (b) Spectral profile and microscopy image of a microLED device-under-test. (c) Microscopy image depicting a fabricated device. (d) Current density versus voltage curves. (e) Measured output power versus current density. (f) Qualitative EQE measurements versus current density.

Optics EXPRESS

within the microLED pixel because current can spread laterally within the microLED before recombination. The same trends observed in Fig. 2 remain consistent if data is plotted by current density where the area is defined as the microLED size instead, this phenomenon is discussed in more detail below. The light grey arrows point in the trend of increasing microLED pixel size to observe luminosity and electrical performance trends. Maximum output power at a current density of 3000 A / cm^2 is 17% greater for the 20 μm microLED when compared to the 10 μm microLED. This is due to a larger amount of the current being able to recombine radiatively rather than through surface recombination. This is illustrated by the trend of increasing IQE with microLED diameter despite the same current. This is elucidated further by examining the amount of recombined surface current, which is vastly higher for the 10 μm microLED and decreases for each larger microLED. The trend observed in Fig. 2(c) and (d) is most prevalent for 10 to 13 μm diameter microLEDs and rolls off at larger diameters where surface recombination current is almost 0 for the largest devices. This suggests that lateral current spreading within the pGaN layer and the emission layer is significant for one to two microns beyond the pGaN contact diameter.

LIV measurements of fabricated devices of the same design and dimensions from SpeCLED modeling are displayed in Fig. 3. Figure 3(a) shows a schematic of the measurement setup where the microLED devices are placed above the power meter and bottom emitted light is collected. Figures 3(b) and (c) show the spectral output and microscopy images of a fabricated device. Figure 3 additionally highlights current-voltage characteristics, measured output power, and qualitative EQE curves. Notably in Fig. 3(e) and (f), the same trends in output power and EQE are observed with increasing die size as seen in Fig. 2. The fabricated devices show a greater difference in power output from the 20 to 10 μm die when compared to the modeled devices with 70% greater power at 2800 A/cm^2 and 83% greater power at the maximum 12,730 A/cm^2 measured current density. The EQE curves in Fig. 3(f) show an increasing peak EQE current density with increasing die size. This is in contrast to the IQE curves in Fig. 2(b) that show decreasing peak IQE current density. There are several factors in our models that could be affecting the peak IQE current density. In particular, the surface recombination velocity and carrier diffusion length were estimated from commonly reported literature values. Modeling results could be improved by empirically solving for these constants for a particular device epitaxy. Both modeled and fabricated results support increased efficiencies by increasing the microLED diameter for a fixed pGaN contact area.

3.2. *Constant microLED Size with variable pGaN contact diameter*

While expanding microLED size for a constant contact geometry improves output power, it is done so at the expense of die real estate. For microLED display applications that require high fill factors, die space for integrated thin-film transistors, tight fabrication tolerances, or extremely small emitters, expanding the microLED pixel may not be a feasible option. This section examines a constant microLED size assuming a fabrication or design requirement and investigates whether there is an optimal pGaN contact diameter that will increase IQE by reducing surface recombination.

Modeled results of varying the pGaN contact diamater with a fixed microLED size are shown in Fig. 4. Current density is calculated for a constant 10 μm microLED diameter size rather than pGaN contact diameter size for comparison consistency. The grey arrow points in the trends observed for increasing pGaN contact diameter. IQE has a negative trend with increasing contact diameter size for lower current densities but the trend reverses at higher current densities. The smaller contacts reach a high-level injection state at lower current densities due to the smaller pGaN contact. Surface recombination current follows an expected trend with smaller pGaN contacts having low or negligible surface recombination at high current densities and larger pGaN contacts are responsible for large surface recombination current loss. Power plots shown

Optics EXPRESS

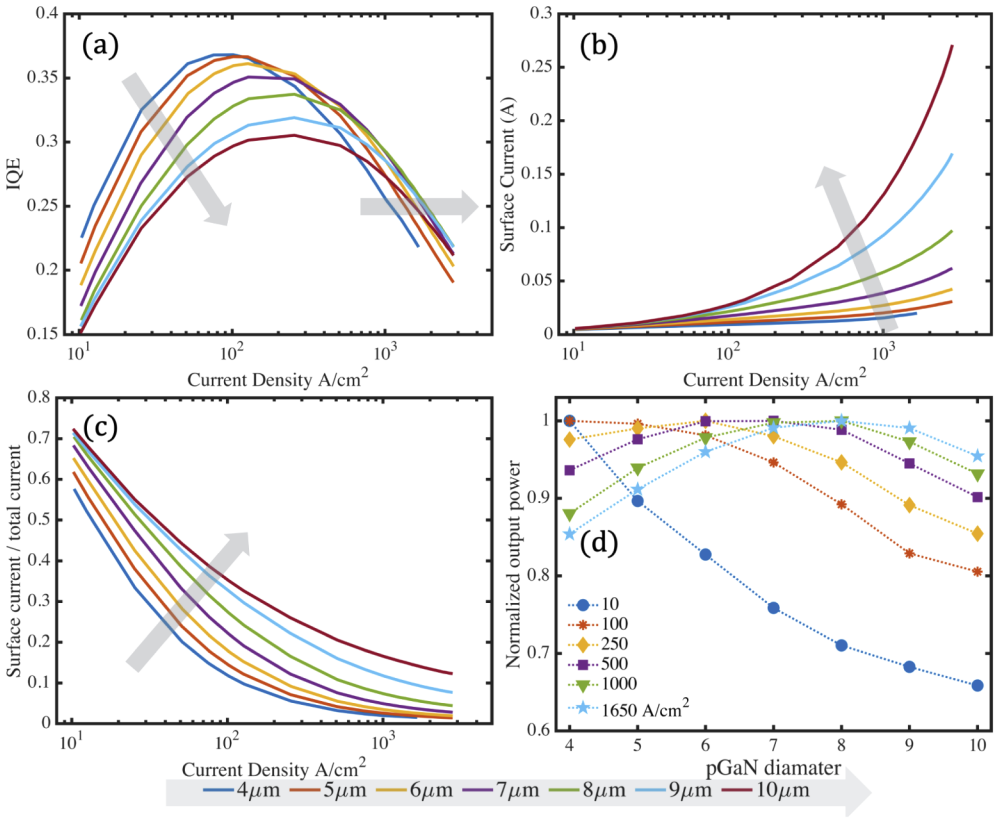

Fig. 4. Modeled device results for microLEDs with a 10 μm diameter and varying pGaN contact diameters as depicted in Fig. 1(d). (a) IQE versus current density. (b) Surface recombination current versus current density. (c) Ratio of surface recombination current to total operational current versus current density. (d) Normalized power output versus pGaN contact diameter plotted for several current densities.

in Fig. 2(a) and 3(c) are not presented here as the output powers for each pGaN diameter were difficult to differentiate. Instead, Fig. 4(d) shows plots of output power versus pGaN diameter for several current densities. Output power for each current density is normalized to the pGaN contact diameter's maximum output power. This plot shows an extraordinary trend where output power can vary significantly (32% different for 10 A/cm^2) with different pGaN contact diameters. The trend is most prominent at lower current densities where a minimum pGaN contact size is preferred. At higher current densities, the trend of maximum output power shifts to larger pGaN contacts. For all current densities though, maximum output power occurs at a pGaN contact diameter of 8 μm or less. This demonstrates that by leaving a 1 μm gap between the pGaN contact perimeter and the microLED edge, surface recombination losses can be substantially suppressed. Given that displays will often operate within target brightness constraints for specific applications, consideration should be given to the the optimal pGaN contact diameter for a fixed microLED size and operational current density.

To detail this phenomenon further, 2D emission power density (W/cm^2) plots of the active emitting area are displayed in Fig. 5. These plots represent how current spreads through the thin (150 nm) pGaN layer into the MQW emitting region with lateral diffusion, the localized IQE, temperature distribution, and surface recombination taken into account. pGaN contact diameters

Optics EXPRESS

of 4, 7, and 10 μm at current densities of 25, 100, and 1000 A/cm^2 are shown as representative points from Fig. 4(d).

For devices operating at low current densities (~25 to 100 A/cm^2), results from Fig. 4(d) show that a minimum pGaN contact size across the ranges examined gives the maximum amount of output power. The smaller contact size creates a higher current density than plotted values at the center of the microLED, pushing the localized IQE higher as depicted from Fig. 4(a). Beyond this, IQE decreases for higher current densities due to current crowding, increased localized temperature, and Auger recombination effects. Additionally, small pGaN contact sizes minimize the amount of surface recombination as the distance from the contact edge to the etched microLED surface is much longer than the carrier diffusion length in pGaN [37–40]. This phenomenon is clearly depicted in Fig. 5(b) for 25 and 100 A/cm^2 where emission power density is highly localized around the center of the microLEDs for the smaller pGaN contact sizes.

At higher current densities, the small contact size becomes less optimal. The localized current density increases, causing the IQE to roll off more rapidly. The smaller pGaN contacts cover far less available emission area and current can not sufficiently spread to the outer radii of the microLED. This is depicted in the 1000 A/cm^2 column of Fig. 5(a) and (b) where there is a strong drop off in power density outside the contact region. This would suggest that a pGaN contact matching the size of the microLED would be optimal to properly distribute current and minimize droop at higher current densities. The main complication is that surface recombination has a negative effect on output power. For high current densities (> 250 A/cm^2), the optimum contact size trends from 6 to 8 μm as current density increases to the maximum density modeled (1650 A/cm^2).

3.3. Device architecture considerations

This work has been focused primarily on efficiency and power output as figures-of-merit as they are generalized and apply to most microLED applications. However, the taxonomy of microLED architectures is vast and rapidly developing, and design constraints for different applications will be able to take the device improvements presented here into consideration. Of particular note, light outcoupling efficiency is largely dependent on device implementation and architecture. This study assumes a constant 30% light extraction efficiency (LEE) to calculate output power from localized IQE and current densities in modeled results. While real results may differ because of the slightly different geometries, the small changes in localized power densities are not significant enough to alter the presented trends. This is validated by the fabricated devices in Fig. 3 following the same trends as the modeled devices in Fig. 2. Further, the fabricated devices show an enhanced trend from the modeled devices, with an output power at 2800 A/cm^2 differed a full 70% from the 10 to 20 μm diameter fabricated microLEDs whereas SpeCLED reuslts only predicted a 17% power difference. This discrepancy can likely be explained from a low estimation of the surface recombination velocity in simulation. Recombination velocities can vary significantly for GaN/InGaN microLEDs depending on epitaxy and etching quality and methods [11]. From this, we can predict that the trends observed in Fig. 4 may be even more pronounced, given further motivation to examine microLED devices with smaller pGaN contact geometries for a constant die diameter.

Outside of figure-of-merit improvements, the second consideration display designers may take into account is the desired beam shape of outcoupled light for the given architecture. A detailed analysis of beam shape would require ray-tracing studies in-situ from emission power density data and is beyond the scope of this study due to the variety of applications that could alter the figures-of-merit. Instead, a shorter discussion on how beam shape could effect different architectures is presented. Larger scale display systems that involve pick-and-place or other mass transfer methodologies are likely outcoupling bottom-emitting light with lesser geometry constraints on die size. Here, the maximum amount of efficiency and output power is desired

Optics EXPRESS

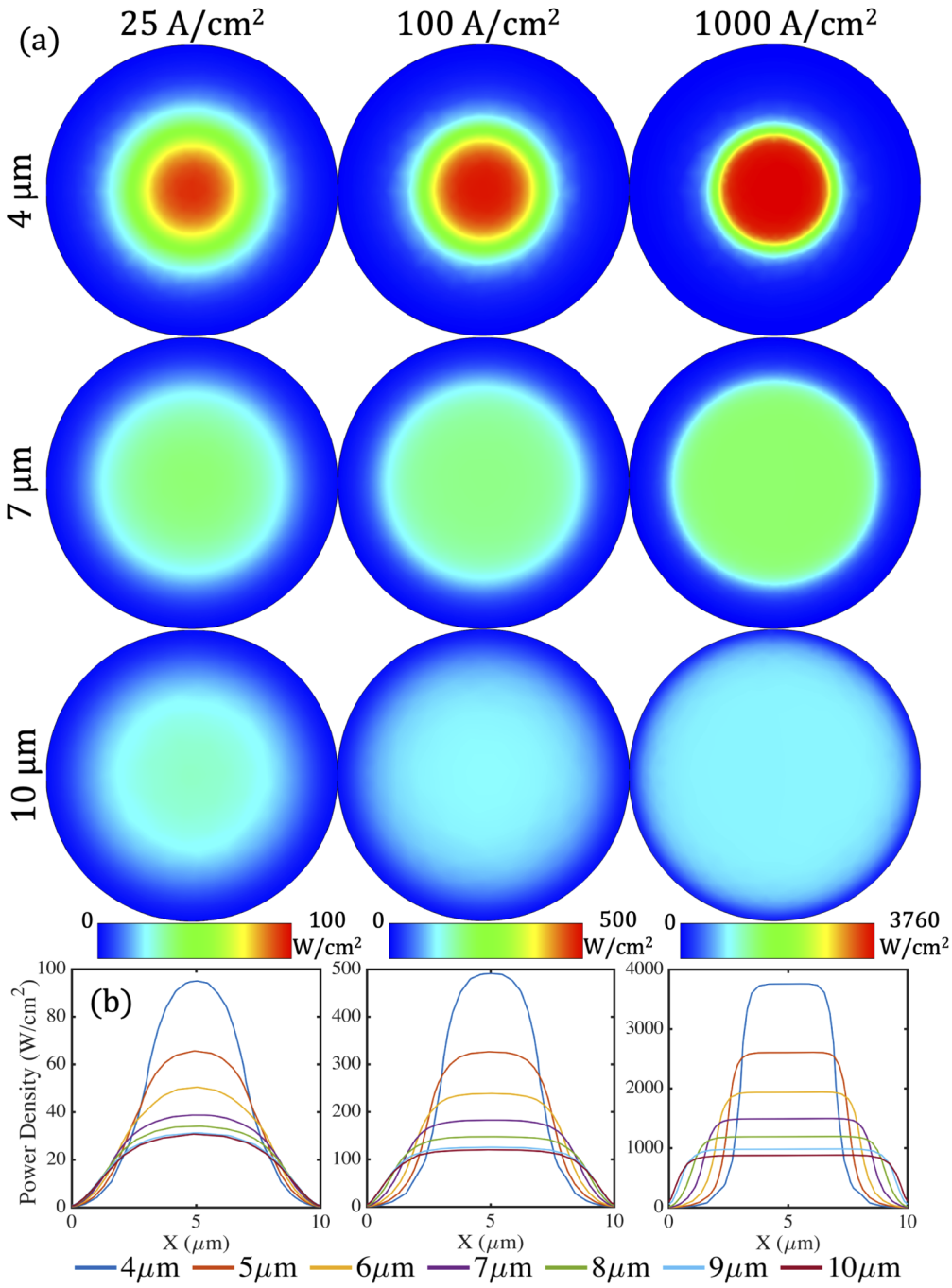

Fig. 5. Power density graphics for microLEDs with a 10 μm diameter. (a) Each row corresponds to the labeled pGaN contact diameter and each column corresponds to a different operational current density where the area is calculated from the total microLED area independent of contact size. (b) Plots on the bottom represent cross-sectional line probes of power density across the center of the microLED for the column's operational current density. All pGaN contact diameters are plotted in each graph.

Optics EXPRESS

and output power can be significantly enhanced by increasing the microLED diameter size as presented in section 2.1. However, this may change the beam shape outcoupled from the bottom of the microLED and could be a less desirable tradeoff for certain applications. The second scenario presented in section 2.2 with a constant microLED diameter and varying pGaN contact sizes is more applicable to monolithic microLED display designs. Here, the driving electronics are integrated directly with the microLED array and device real-estate is at a premium. There is a careful balance in maximizing microLED fill-factor, reducing interconnect resistance, and ample channel width for high current driving capabilities to consider. The results here suggest power output can be improved by carefully selecting a pGaN contact size for a display's driving current density. Finally, due to the small amount of lateral current spreading in the pGaN and the emission area as depicted by Fig. 5(b), the beam shape of top-emitting devices are strongly dependent on the top-contact geometry. Therefore, a simple method to decrease the apparent pixel size is to reduce the shape of the contact geometry without necessarily etching the microLED shape to match. This both simplifies fabrication methods and improves quantum efficiency of the device.

4. Conclusion

This study demonstrates significant efficiency improvements through modeling and fabricated devices by a novel method of reshaping pGaN contact geometries to reduce surface recombination. Different contact geometries alter the current densities for a given microLED size and can be harnessed to maximize efficiency for a target display brightness. Display designers should carefully consider the balance between current density, brightness, efficiency, and beam shape characteristics to optimize the pGaN contact shape rather than use a self-aligned microLED design.

Funding. National Science Foundation (1926747); National Institutes of Health (5R21EY029458-02).

Acknowledgments. We would like to thank STR Group for their assistance and advice on device modeling. In particular, special thanks to Kirill Bulashevich for your help in model optimization and design. Additional thanks to Magic Leap for providing grant funding to partially sponsor this project. This work was carried out in part in the Clean room / Electron Microscopy / Shared Materials Characterization/ lab of Columbia Nano Initiative (CNI) Shared Lab Facilities at Columbia University.

Disclosures. The authors declare no conflicts of interest.

Data availability. Data underlying the results presented in this paper are not publicly available at this time but may be obtained from the authors upon reasonable request.

References

1. Y. Huang, E.-L. Hsiang, M.-Y. Deng, and S.-T. Wu, "Mini-LED, Micro-LED and OLED displays: present status and future perspectives," Light: Sci. Appl. **9**(1), 105 (2020).
2. X. Zhou, P. Tian, C.-W. Sher, J. Wu, H. Liu, R. Liu, and H.-C. Kuo, "Growth, transfer printing and colour conversion techniques towards full-colour micro-LED display," Prog. Quantum Electron. **71**, 100263 (2020).
3. Z. Liu, C.-H. Lin, B.-R. Hyun, C.-W. Sher, Z. Lv, B. Luo, F. Jiang, T. Wu, C.-H. Ho, H.-C. Kuo, and J.-H. He, "Micro-light-emitting diodes with quantum dots in display technology," Light: Sci. Appl. **9**(1), 83 (2020).
4. F. Olivier, S. Tirano, L. Dupré, B. Aventurier, C. Largeron, and F. Templier, "Influence of size-reduction on the performances of GaN-based micro-LEDs for display application," J. Lumin. **191**, 112–116 (2017).
5. W. Tian and J. Li, "Size-dependent optical-electrical characteristics of blue GaN/InGaN micro-light-emitting diodes," Appl. Opt. **59**(29), 9225 (2020).
6. K. A. Bulashevich and S. Y. Karpov, "Is Auger recombination responsible for the efficiency rollover in III-nitride light-emitting diodes?" Phys. Status Solidi C **5**(6), 2066–2069 (2008).
7. Z. Gong, S. Jin, Y. Chen, J. McKendry, D. Massoubre, I. M. Watson, E. Gu, and D. Dawson, "Size-dependent light output, spectral shift, and self-heating of 400 nm InGaN light-emitting diodes," J. Appl. Phys. **107**(1), 013103 (2010).
8. C. Shen, T. K. Ng, Y. Yang, D. Cha, and B. S. Ooi, "InGaN micro-LED-pillar as the building block for high brightness emitters," in *2013 IEEE Photonics Conference*, (IEEE, Bellevue, WA, USA, 2013), pp. 174–175.
9. A. Daami, F. Olivier, L. Dupré, F. Henry, and F. Templier, "59-4: *Invited Paper:* Electro-optical size-dependence investigation in GaN micro-LED devices," SID Symp. Dig. Tech. Pap. **49**(1), 790–793 (2018).
10. F. Olivier, A. Daami, C. Licitra, and F. Templier, "Shockley-Read-Hall and Auger non-radiative recombination in GaN based LEDs: A size effect study," Appl. Phys. Lett. **111**(2), 022104 (2017).

Optics EXPRESS

11. K. A. Bulashevich and S. Y. Karpov, "Impact of surface recombination on efficiency of III-nitride light-emitting diodes," Phys. Status Solidi RRL - Rapid Res. Lett. **10**(6), 480–484 (2016).
12. X. A. Cao, S. J. Pearton, A. P. Zhang, G. T. Dang, F. Ren, R. J. Shul, L. Zhang, R. Hickman, and J. M. Van Hove, "Electrical effects of plasma damage in p-GaN," Appl. Phys. Lett. **75**(17), 2569–2571 (1999).
13. S. Pearton, R. J. Shul, and F. Ren, "A Review of Dry Etching of GaN and Related Materials," MRS Internet J. Nitride Semicond. Res. **5**(1), e11 (2000).
14. F. A. Khan, L. Zhou, V. Kumar, and I. Adesida, "Plasma-induced damage study for n-GaN using inductively coupled plasma reactive ion etching," J. Vac. Sci. Technol., B: Microelectron. Process. Phenom. **19**(6), 2926 (2001).
15. J.-M. Lee, K.-M. Chang, I.-H. Lee, and S.-J. Park, "Cl 2 -Based Dry Etching of GaN and InGaN Using Inductively Coupled Plasma - The Effects of Gas Additives," J. Electrochem. Soc. **147**(5), 1859 (2000).
16. S. J. Pearton, J. C. Zolper, R. J. Shul, and F. Ren, "GaN: Processing, defects, and devices," J. Appl. Phys. **86**(1), 1–78 (1999).
17. N. Okada, K. Nojima, N. Ishibashi, K. Nagatoshi, N. Itagaki, R. Inomoto, S. Motoyama, T. Kobayashi, and K. Tadatomo, "Formation of distinctive structures of GaN by inductively-coupled-plasma and reactive ion etching under optimized chemical etching conditions," AIP Adv. **7**(6), 065111 (2017).
18. W. H. Choi, G. You, M. Abraham, S.-Y. Yu, J. Liu, L. Wang, J. Xu, and S. E. Mohney, "Sidewall passivation for InGaN/GaN nanopillar light emitting diodes," J. Appl. Phys. **116**(1), 013103 (2014).
19. M. S. Wong, D. Hwang, A. I. Alhassan, C. Lee, R. Ley, S. Nakamura, and S. P. DenBaars, "High efficiency of III-nitride micro-light-emitting diodes by sidewall passivation using atomic layer deposition," Opt. Express **26**(16), 21324 (2018).
20. J. Piprek, "Efficiency droop in nitride-based light-emitting diodes: Efficiency droop in nitride-based light-emitting diodes," Phys. Status Solidi A **207**(10), 2217–2225 (2010).
21. J. Cho, E. F. Schubert, and J. K. Kim, "Efficiency droop in light-emitting diodes: Challenges and countermeasures: Efficiency droop in light-emitting diodes: Challenges and countermeasures," Laser Photonics Rev. **7**(3), 408–421 (2013).
22. E. Kioupakis, Q. Yan, D. Steiauf, and C. G. Van de Walle, "Temperature and carrier-density dependence of Auger and radiative recombination in nitride optoelectronic devices," New J. Phys. **15**(12), 125006 (2013).
23. D. S. Meyaard, G.-B. Lin, J. Cho, E. Fred Schubert, H. Shim, S.-H. Han, M.-H. Kim, C. Sone, and Y. Sun Kim, "Identifying the cause of the efficiency droop in GaInN light-emitting diodes by correlating the onset of high injection with the onset of the efficiency droop," Appl. Phys. Lett. **102**(25), 251114 (2013).
24. I. E. Titkov, S. Y. Karpov, A. Yadav, V. L. Zerova, M. Zulonas, B. Galler, M. Strassburg, I. Pietzonka, H.-J. Lugauer, and E. U. Rafailov, "Temperature-Dependent Internal Quantum Efficiency of Blue High-Brightness Light-Emitting Diodes," IEEE J. Quantum Electron. **50**(11), 911–920 (2014).
25. J. Li, B. Ma, R. Wang, and L. Han, "Study on a cooling system based on thermoelectric cooler for thermal management of high-power LEDs," Microelectron. Reliab. **51**(12), 2210–2215 (2011).
26. J. Li, X. Zhang, C. Zhou, J. Zheng, D. Ge, and W. Zhu, "New Applications of an Automated System for High-Power LEDs," IEEE/ASME Trans. Mechatron **21**(2), 1035–1042 (2016).
27. E. F. Schubert, *Light-Emitting Diodes* (Cambridge University, 2006), 2nd ed.
28. S. Karpov, "ABC-model for interpretation of internal quantum efficiency and its droop in III-nitride LEDs: a review," Opt. Quantum Electron. **47**(6), 1293–1303 (2015).
29. D. S. Y. Hsu, C. S. Kim, C. R. Eddy, R. T. Holm, R. L. Henry, J. A. Casey, V. A. Shamamian, and A. Rosenberg, "Using Ni masks in inductively coupled plasma etching of high density hole patterns in GaN," J. Vac. Sci. Technol., B: Microelectron. Process. Phenom. **23**(4), 1611 (2005).
30. J.-S. Jang, I.-S. Chang, H.-K. Kim, T.-Y. Seong, S. Lee, and S.-J. Park, "Low-resistance Pt/Ni/Au ohmic contacts to *p* -type GaN," Appl. Phys. Lett. **74**(1), 70–72 (1999).
31. J. K. Sheu, Y. K. Su, G. C. Chi, P. L. Koh, M. J. Jou, C. M. Chang, C. C. Liu, and W. C. Hung, "High-transparency Ni/Au ohmic contact to *p* -type GaN," Appl. Phys. Lett. **74**(16), 2340–2342 (1999).
32. P. Shyi-Ming, T. Ru-Chin, F. Yu-Mei, Y. Ruey-Chyn, and H. Jung-Tsung, "Enhanced output power of InGaN-GaN light-emitting diodes with high-transparency nickel-oxide-indium-tin-oxide Ohmic contacts," IEEE Photonics Technol. Lett. **15**(5), 646–648 (2003).
33. H.-H. Hu and A. Bibl, "Method of Forming a Micro LED Device with Self-Aligned Metallization Stack," (2017).
34. H. Kim, K.-K. Kim, K.-K. Choi, H. Kim, J.-O. Song, J. Cho, K. H. Baik, C. Sone, Y. Park, and T.-Y. Seong, "Design of high-efficiency GaN-based light emitting diodes with vertical injection geometry," Appl. Phys. Lett. **91**(2), 023510 (2007).
35. K. A. Bulashevich, S. S. Konoplev, and S. Y. Karpov, "Effect of Die Shape and Size on Performance of III-Nitride Micro-LEDs: A Modeling Study," Photonics **5**(4), 41 (2018).
36. S. S. Konoplev, K. A. Bulashevich, and S. Y. Karpov, "From Large-Size to Micro-LEDs: Scaling Trends Revealed by Modeling," Phys. Status Solidi A **215**(10), 1700508 (2018).
37. J. C. Gonzalez, K. L. Bunker, and P. E. Russell, "Minority-carrier diffusion length in a GaN-based light-emitting diode," Appl. Phys. Lett. **79**(10), 1567–1569 (2001).
38. K. Kumakura, T. Makimoto, N. Kobayashi, T. Hashizume, T. Fukui, and H. Hasegawa, "Minority carrier diffusion length in GaN: Dislocation density and doping concentration dependence," Appl. Phys. Lett. **86**(5), 052105 (2005).

Optics EXPRESS

39. T. Malinauskas, R. Aleksiejunas, K. Jarašiunas, B. Beaumont, P. Gibart, A. Kakanakova-Georgieva, E. Janzen, D. Gogova, B. Monemar, and M. Heuken, "All-optical characterization of carrier lifetimes and diffusion lengths in MOCVD-, ELO-, and HVPE- grown GaN," J. Cryst. Growth **300**(1), 223–227 (2007).
40. E. Yakimov, "What is the real value of diffusion length in GaN?" J. Alloys Compd. **627**, 344–351 (2015).